remote sensing

MDPI

Article

A Deep Learning Application for Deformation Prediction from Ground-Based InSAR

Jianfeng Han [1], Honglei Yang [1,*], Youfeng Liu [1], Zhaowei Lu [1], Kai Zeng [1] and Runcheng Jiao [2]

[1] School of Land Science and Technology, China University of Geosciences, Beijing 100083, China
[2] Beijing Institute of Geological Hazard Prevention, Beijing 100120, China
* Correspondence: hongleiyang@cugb.edu.cn

Abstract: Ground-based synthetic aperture radar interferometry (GB-InSAR) has the characteristics of high precision, high temporal resolution, and high spatial resolution, and is widely used in highwall deformation monitoring. The traditional GB-InSAR real-time processing method is to process the whole data set or group in time sequence. This type of method takes up a lot of computer memory, has low efficiency, cannot meet the timeliness of slope monitoring, and cannot perform deformation prediction and disaster warning forecasting. In response to this problem, this paper proposes a GB-InSAR time series processing method based on the LSTM (long short-term memory) model. First, according to the early monitoring data of GBSAR equipment, the time series InSAR method (PS-InSAR, SBAS, etc.) is used to obtain the initial deformation information. According to the deformation calculated in the previous stage and the atmospheric environmental parameters monitored, the LSTM model is used to predict the deformation and atmospheric delay at the next time. The phase is removed from the interference phase, and finally the residual phase is unwrapped using the spatial domain unwrapping algorithm to solve the residual deformation. The predicted deformation and the residual deformation are added to obtain the deformation amount at the current moment. This method only needs to process the difference map at the current moment, which greatly saves time series processing time and can realize the prediction of deformation variables. The reliability of the proposed method is verified by ground-based SAR monitoring data of the Guangyuan landslide in Sichuan Province.

Keywords: GB-InSAR; LSTM model; deformation prediction; real-time processing

Citation: Han, J.; Yang, H.; Liu, Y.; Lu, Z.; Zeng, K.; Jiao, R. A Deep Learning Application for Deformation Prediction from Ground-Based InSAR. *Remote Sens.* **2022**, *14*, 5067. https://doi.org/10.3390/rs14205067

Academic Editors: Alex Hay-Man Ng, Linlin Ge, Hsing-Chung Chang and Zheyuan Du

Received: 2 August 2022
Accepted: 1 October 2022
Published: 11 October 2022

1. Introduction

After 20 years of continuous development of ground-based SAR, many scholars and experts have conducted research on its application in different fields, so that ground-based SAR can continue to develop and be suitable for monitoring in different scenarios [1–5]. In 2018, S. Kuraoka successfully monitored the eruption process of Hakone volcano in Japan using the IBIS-L system, proving that GB-InSAR technology is a feasible method for monitoring volcanic activity [6]. In 2018, in order to study the relationship between the evolution of volcanic landforms and slope instability, Di Traglia et al. used the joint monitoring method of COSMO satellite and ground-based SAR to monitor volcanoes in a certain area of Italy. This method emphasized ground-based SAR equipment and spaceborne SAR. The feasibility of joint monitoring volcanic activity provides a feasible method for the subsequent study of volcanic evolution [7]. In 2019, T.carla et al. adopted the method of joint GNSS, spaceborne SAR and ground-based SAR for a landslide in the alpine region of Italy; the experiment proved the feasibility of the joint measurement of GNSS technology and InSAR technology, and has more advantages for GNSS technology in snow-covered areas, which provides ideas and methods for subsequent joint data and InSAR monitoring in alpine regions [8]. In 2021, T. Carla et al. used GB-InSAR technology to process and analyze the monitoring data of a large landslide in the Italian Alps for ten years, and

analyzed the impact of hydrological changes on the surface deformation rate by combining with precipitation and snowfall data, and constructed a finite element method. The model models the deformation rate of the landslide mass at different heights and depths, and experiments demonstrate the importance of long-term GB-InSAR monitoring [9].

GB-InSAR has a higher sampling frequency, which can describe the dynamic deformation process of the monitoring target more finely [10–15]. The high sampling frequency also brings the problem of a large amount of data. How to quickly calculate the deformation-monitoring results is a hot issue in current research, which is of great significance to the early warning and prediction of geological disasters. The current GB-InSAR time series methods mainly use permanent scatterer technology and small baseline set technology. According to the idea of statistics, modeling and analysis are carried out for points that maintain stable and reliable phase quality in the time dimension, and finally the time series monitoring results of the points are obtained. However, these methods require analysis of the entire data set which is inefficient, and with the accumulation of data, the hardware requirements are also high, and the future cannot be predicted, which is not conducive to the prevention and control of geological disasters. In recent years, China and other countries have also carried out relevant research. In 2019, Wang proposed a real-time ground-based synthetic aperture radar processing method [16], (real-time ground-based SAR, RT-GBSAR), which is based on SBAS-InSAR. The data set is divided into different units for processing, which has the characteristics of small system resource occupation and fast processing. Izumi et al. adopted the method of packet processing [17] to realize real-time data processing. Group processing solves the problem of real-time processing to a certain extent, but it does not have the function of deformation prediction, and there are still certain limitations in the monitoring of ground disasters.

Long short-term memory (LSTM) is an improvement in the recurrent neural network (RNN) model, which solves the phenomenon of gradient disappearance and gradient explosion, and can be used to solve the problem of long-term sequence prediction problems. In recent years, the LSTM model has also been used in InSAR data processing. In 2021, Liu Qinghao et al. built an LSTM model to predict the land subsidence results obtained by InSAR time series processing. However, the application of combining the LSTM model with GB-InSAR to realize deformation prediction and real-time processing is seldom [18]. GB-InSAR has high frequency and regular sampling frequency, so it is suitable to use the LSTM model for time series analysis.

Aiming at the problems of high resource occupation, long consumption time and poor prediction effect in GB-InSAR time series data processing, this paper proposes a real-time GB-InSAR slope deformation processing method based on the LSTM model. The first step is to build a deep learning sample library for the deformation variables obtained in the pre-processing, then to train the LSTM deep learning model, use the LSTM model to predict the deformation variables at the next moment, and remove them from the current differential phase. At the same time, the deep learning sample library is constructed for the atmospheric parameters obtained in the previous stage, the training model is used, and the atmospheric phase at the next moment is predicted, and the same is removed from the current differential phase. Finally, the residual phase is unwrapped using the spatial domain unwrapping algorithm, and the residual deformation is calculated. The predicted deformation and the residual deformation are added to obtain the deformation amount at the current moment. This method only needs to process the difference map at the current moment, which greatly saves time series processing time and can realize the prediction of deformation variables.

2. Materials and Methods

2.1. Desciption of Guangyuan Landslides

On 7 October 2021, a landslide occurred near Yanwo Village, Guangyuan City, Sichuan Province. The landslide was located near Dashiyan, Yanwo Village, Guangyuan City, specifically at 106°0′41.53″ east longitude, 32°22′28.449″ north latitude. The highest point

is located on the top of the mountain in the north, with an altitude of 756 m, and the lowest point is located at the bottom of the mountain, with an altitude of 540m, and the height difference between the two is 216 m. The upper part of the landslide is steep, with a gradient of about 15° to 30°, and the lower part is relatively gentle, with a gradient of about 5° to 20°, and the overall main sliding direction is about 223°. The landslide starts from the upper part of the hillside, the trailing edge of the landslide is bounded by bedrock, and the west and east sides are bounded by a little exposed bedrock. The possibility of the landslide continuing to expand cannot be ruled out. The landslide is about 851 m long, 120 m to 160 m wide, about 2 m thick on average, and has a distribution area of about 77,297 square meters. It is a large soil landslide. The landslide extends in the southwest direction as a whole, and the lateral extension is short. At present, the deformation of the landslide is mainly concentrated in the top trailing edge, local slow displacement occurs at the soil layer accumulation from the middle to the bottom, and the overall structure tends to be stable. If the landslide deforms significantly and this causes the landslide to become unstable, then the landslide will pose a threat to the residents in the danger zone and the three high-voltage power line towers. Contact monitoring is dangerous, and the satellite time baseline is long, which is not suitable for emergency monitoring. Therefore, GB-InSAR with short time baseline, high resolution and flexible observation angle is used for continuous monitoring. The location of the study area and the field equipment is shown in Figure 1.

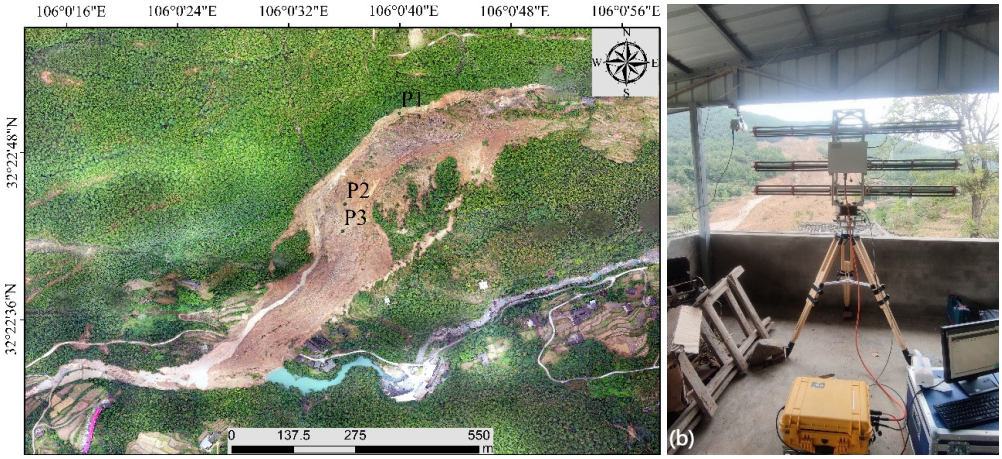

Figure 1. (**a**) is an orthophoto image processed by the DJI Royal 2 drone on 30 October 2021, showing the geographic location of the study area. P1, P2 and P3 are three study points selected from different locations of the landslide. P1 is the rear wall of the landslide, P2 is the landslide platform, and P3 is the secondary step. (**b**) is a photo of the GPRI-II equipment and the landslide mass.

The GAMMA Portable Radar Interferometer (GPRI-II) was set up 500 m south of the landslide. At the same time, the FSR-8 automatic weather station with the same time baseline was used to collect the necessary meteorological parameters for a total of 16 days, of which there was no interruption in the first 14 days. Day 15 was suspended for 8 h due to power issues. The main parameters during measurement are show in Table 1:

Table 1. SAR data acquisition parameters.

Radar elevation angle	0°
Radar gain	54 dB
Measuring distance range	30 m–1400 m
Measuring angle range	−90°–60°
Range resolution	0.7495 m
Azimuth resolution (−3 dB)	6.8 m (1 km)
Single imaging time	15 s
Time interval between two images	5 min

2.2. GB-InSAR Phase Model

After GBSAR was installed, the monitoring target was observed at a certain frequency (minute level). Due to the stable observation attitude, a zero baseline could be achieved. Compared with the spaceborne interference phase model, there is no reference plane phase and elevation phase, and the corresponding interference phase model can be represented by the following formula:

$$\varphi = \varphi_{def} + \varphi_{atm} + \varphi_{noise} + 2k\pi \tag{1}$$

Among them, φ is the interferometric phase of the wrapping, φ_{def} is the deformation corresponding to the radar line of sight, φ_{atm} is the atmospheric delay phase in the radar line of sight, φ_{noise} is the interference phase noise, and k is the number of integer cycles [19]. Among them, the atmospheric delay phase is the most important error source affecting the monitoring accuracy of GB-InSAR. The research shows that at a distance of 1 km from the GBSAR device, when the temperature is 20 °C, a 1% humidity change can lead to a measurement error of 2 mm [20,21].

According to the propagation mode of electromagnetic waves in the air, a mathematical model and a physical model were constructed for the atmospheric delay phase. The mathematical model is based on the propagation principle of electromagnetic waves. The radar emits electromagnetic waves with a wavelength of 1 at all times, and the electromagnetic waves reach the target pixel after the propagation distance return. The echo phase model for this pixel is [22]:

$$\varphi_p(i,j) = \frac{4\pi}{\lambda}\int_0^{r(i,j)} n(r,t)dr \tag{2}$$

n is the refractive index related to distance and time.

The physical model assumes that in the ground-based SAR monitoring, the spatial distribution of the atmospheric medium is assumed to be uniform within the monitoring area of 300–500 m, and the refractive index is independent of distance and only related to time, so the atmospheric phase of the pixel can be expressed as:

$$\varphi(t) = \frac{4\pi r \cdot n(t)}{\lambda} \tag{3}$$

In the formula, the relationship between the refractive index n and the refractive index N can be expressed as:

$$N = (n-1) \times 10^6 \tag{4}$$

In atmospheric refraction studies, the refractive index is usually expressed by temperature, air pressure, and relative humidity [23]:

$$N = \frac{0.2589}{T} + \frac{3.73 \times 10^5 \times e}{T^2} + \frac{71.7 \times e}{T} \tag{5}$$

In the formula, h is the atmospheric pressure and e is the water vapor pressure, which can be expressed as [24] according to the Magnus saturated water vapor pressure formula:

$$e = \frac{h}{100} e_{sat} \tag{6}$$

$$e_{sat} = 6.1016 \cdot 10^{\left(\frac{7.5 \times T}{T+237.3}\right)} \tag{7}$$

Through the above analysis, the range-to-homogeneous atmospheric phase during GBSAR monitoring can be modeled and eliminated from the interference phase, while reducing the difficulty of phase unwrapping in the space domain.

2.3. Long Short-Term Memory for Sequence Modeling

For the phenomenon of gradient disappearance and gradient explosion in RNN, Hochreiter proposed a network structure to improve the gradient disappearance problem, which works in a similar way to RNN. The difference is that a memory storage mechanism is established in some units within RNN to achieve more effective information storage and updates. Figure 2 shows the internal structure of the LSTM. By analyzing Figure 2, it can be seen that LSTM is obviously different from RNN in that it adds a gating unit, and the network transmits the gating unit information and the cell state at the last moment to the next unit in the network.

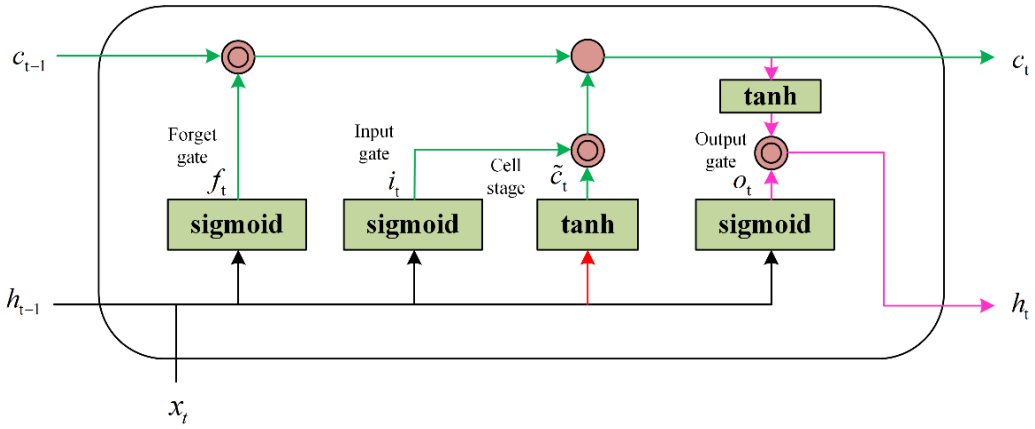

Figure 2. Schematic diagram of the LSTM cell structure. There are four types of gating units in LSTM cells: Forget gate, Input gate, Cell stage and Output gate. c_t and c_{t-1} are the state of the cell at time t and time $t-1$. h_t and h_{t-1} are the state of the hide at time t and time $t-1$. x_t is the input variable at time t.

After the input data are processed by the LSTM model, the predicted value at the next moment is obtained. The LSTM model can be expressed as:

$$f_t = \sigma\left(W_f \cdot [h_{t-1}, x_t] + b_f\right) \tag{8}$$

$$i_t = \sigma(w_i \cdot [h_{t-1}, x_t] + b_i) \tag{9}$$

$$\widetilde{C}_t = \tanh(W_C \cdot [h_{t-1}, x_t] + b_c) \tag{10}$$

$$C_t = f_t \times C_{t-1} + \mathrm{i} \times \widetilde{C}_t \tag{11}$$

$$o_t = \sigma(W_O \cdot [h_{t-1}, x_t] + b_o) \tag{12}$$

$$h_t = o_t \times \tanh(C_t) \tag{13}$$

3. Proposed Methodology

Firstly, this paper uses the time-series InSAR technology to obtain the deformation variable data set, and organizes and models the meteorological parameter data to obtain the atmospheric phase data set. After that, the LSTM prediction model is trained with two kinds of data sets, and the prediction accuracy of the model is evaluated by the prediction effect of the two kinds of data. Finally, the prediction model is used to realize the real-time processing of GB-InSAR monitoring and obtain the real-time processing results. The accuracy of the method is evaluated by the precision of inner coincidence and a computational efficiency evaluation. The technical roadmap for this paper is shown in the Figure 3 below:

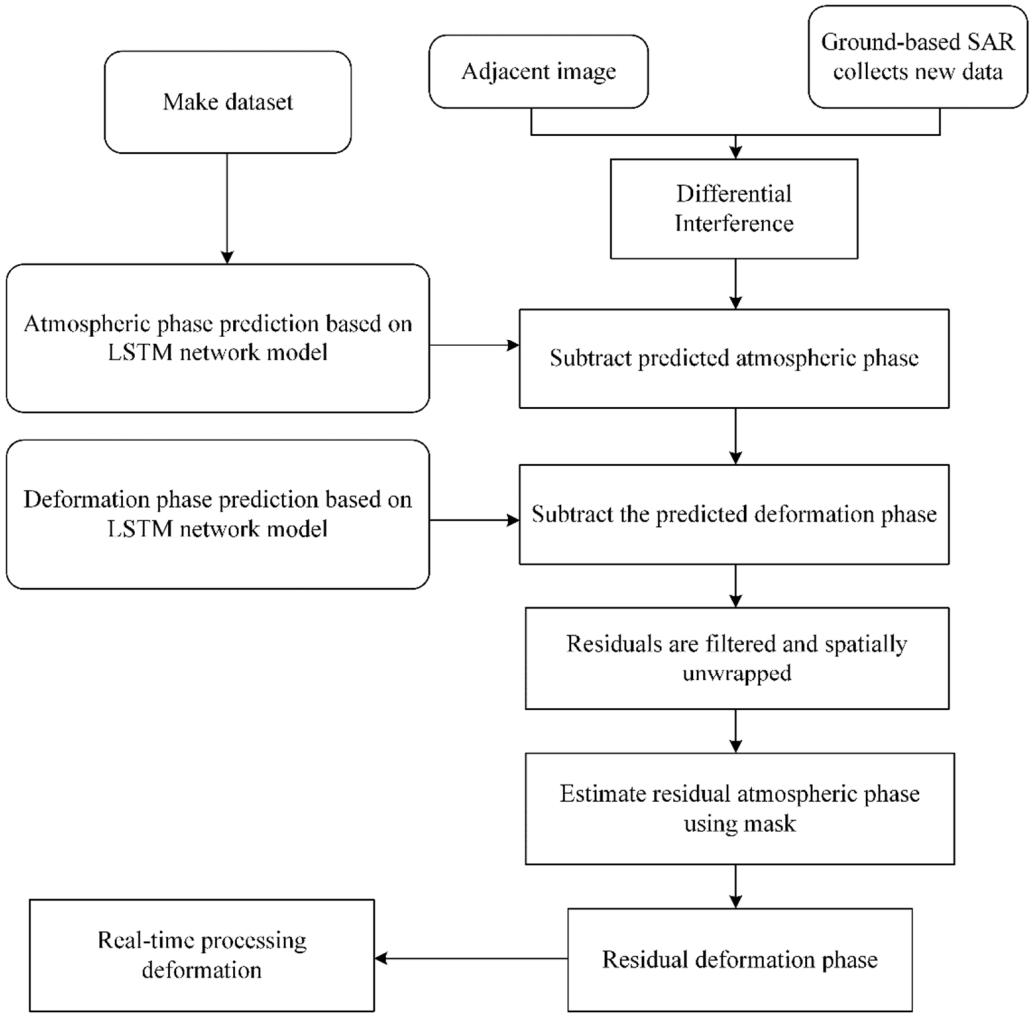

Figure 3. The technical roadmap of GB-InSAR time series processing method based on LSTM model.

3.1. Deformation Prediction

3.1.1. Data Normalization

In order to make the neural network model converge faster and obtain higher prediction accuracy, the variable values entering the neural network model should belong to the same range; that is, the value range of the data set should be consistent, and it is necessary to manually adjust the range of variables according to a certain ratio, the variable is scaled, and the following are two common processing methods:

Normalization refers to the scaling of variable values in the range zero to one or negative one to one [24]. First, make the difference between the maximum value X_{max} and the minimum value of the variable X_{min} to obtain the variation range of the variable X, and then divide each observation X_i value in the variable X with the minimum value X_{min} of the variable X and divide it by the variation range of the variable X to scale the observed value X_i to zero to one; the process is called maximum and minimum normalization, as shown in the following formula:

$$X_{i(nonralized)} = \frac{X_i - X_{min}}{X_{max} - X_{min}} \quad (14)$$

The normalized atmospheric phase value and deformation phase value are selected and shown in Tables 2 and 3.

Table 2. After normalization of deformation data.

Num \ Time	2021.10.17 16:13:05	2021.10.17 16:33:05	2021.10.17 16:53:05	2021.10.17 17:13:05	2021.10.17 17:33:05
1	0.875	0.884	0.885	0.858	0.842
2	0.875	0.882	0.852	0.837	0.839
3	0.875	0.880	0.881	0.858	0.845
4	0.875	0.876	0.878	0.858	0.848

Table 3. After normalization of atmospheric phase data.

Unit \ Time	2021.10.17 16:13:05	2021.10.17 16:33:05	2021.10.17 16:53:05	2021.10.17 17:13:05	2021.10.17 17:33:05
Radian	0.695	0.696	0.686	0.702	0.685

3.1.2. LSTM Network Design

The data set is divided into a training set, validation set and test set according to the ratio of 6:2:2. After the network design is completed, the training set can be input to train the model. In the training process of the model, due to the complex network structure of the neural network, as the number of iterations increases, the model is prone to overfitting. Therefore, in order to have a high generalization ability of the model and avoid overfitting, the model's dropout layer needs to be added in the LSTM layer. The main function of this layer is to discard the neurons in the LSTM layer according to a certain proportion in each training [25].

After experimental testing, the increase in the number of LSTM layers does not change the prediction accuracy of the model, and the selection of timesteps is equally important. Selecting timesteps is three, that is, predicting the deformation variables at the next moment according to the deformation variables of the first three moments, which corresponds to the experiment in this paper. That is, it is recommended to use the one-hour deformation data to predict the deformation data after 20 min as the output. The Units parameter in the LSTM layer represents the number of neurons in this layer, which is the tensor output dimension of the LSTM layer. Activation represents the activation function method. The ReLU activation function is selected in the LSTM layer, and the sigmoid activation function is selected in the Dense layer. This combination method enables the model to obtain higher accuracy. The dropout layer is set to zero point two, that is, twenty percent of neurons are randomly dropped during each training [26–28].

3.1.3. Hyperparameter Selection

For neural network models, there are many hyperparameters in the model, which control the structure, function, and efficiency of the model, and are the key to obtaining high-precision results for the model. The hyperparameter selection of the model in the experiment in this paper is adjusted using the grid search method. By setting the range of hyperparameters, the model is evaluated according to a certain growth rate of hyperparameters, so as to select the combination of hyperparameters with the best model performance.

In the evaluation index of the model, we use the loss rate to measure; the loss rate is mainly the calculation method of the MSE (mean square error), and its calculation method is shown in the following:

$$\mathrm{MSE} = \sum_{i=1}^{n} \frac{(\mathrm{Predicted_i} - \mathrm{Actual_i})^2}{n} \tag{15}$$

In the training process of the model, the fitting degree of the model is judged by measuring the size of the loss function. When the loss rates of the training set and the validation set finally reach the same level, it proves that the model has achieved a good

fitting effect. The combination of hyperparameters of the model determined using the grid search method is shown in Table 4:

Table 4. LSTM model hyperparameter combination table.

Hyperparameter Name	Value
LSTM_units	128
Dropout	0.2
Batch_size	128
epochs	400

For deformable data, this paper conducts first-order difference to remove the autocorrelation of the data itself and then trains the model. For atmospheric phase data, since the data itself have periodic components, this paper uses the STL (seasonal trend loss) method to decompose the periodic term, trend term and residual term. After that, the three components are modeled separately. The predicted values of the three components are then added to obtain the overall predicted value. The training set and validation set loss rate curves of the model are shown in Figures 4 and 5:

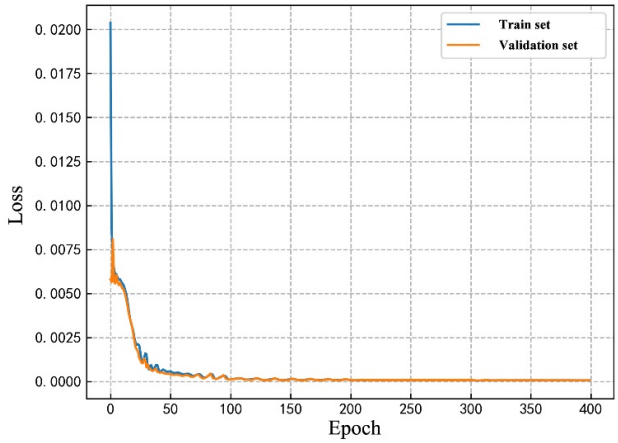

Figure 4. The deformation loss rate curve of the training set and the validation set. The loss value approaches 0 after 400 epochs.

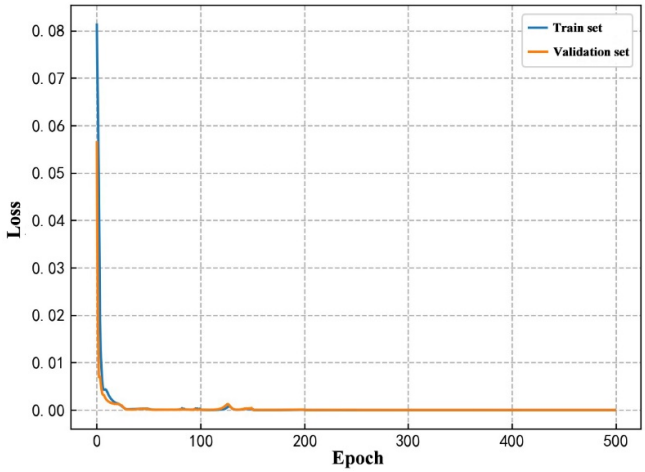

Figure 5. The atmosphere phase loss rate curve of the training set and the validation set. The loss value approaches 0 after 500 epochs.

In the Figure 5, the horizontal axis represents the epoch, and the vertical axis represents the size of the model loss. When the epoch reaches 500 times, the loss rate converges well,

and finally reaches a stable value near 0.000002, indicating that the prediction accuracy of the deformation prediction model is very high.

3.2. Real-Time Processing

3.2.1. Obtaining the Initial Deformation Value

PS-InSAR technology is a method of selecting PS (Permanent Scatterer) point targets for time series analysis by statistically analyzing the SAR time series data in the study area according to the amplitude and phase. Different from the D-InSAR method [29], it only models and analyzes point targets with high coherence, strong scattering and stability, which effectively reduces the impact of decoherence on data processing. Sequence analysis can clearly obtain the change in the deformation of the target area over time, and more intuitively understand the change trend of the surface, which is helpful for the investigation and prevention of geological disasters. The technical process of PS-InSAR is shown in Figure 6 below:

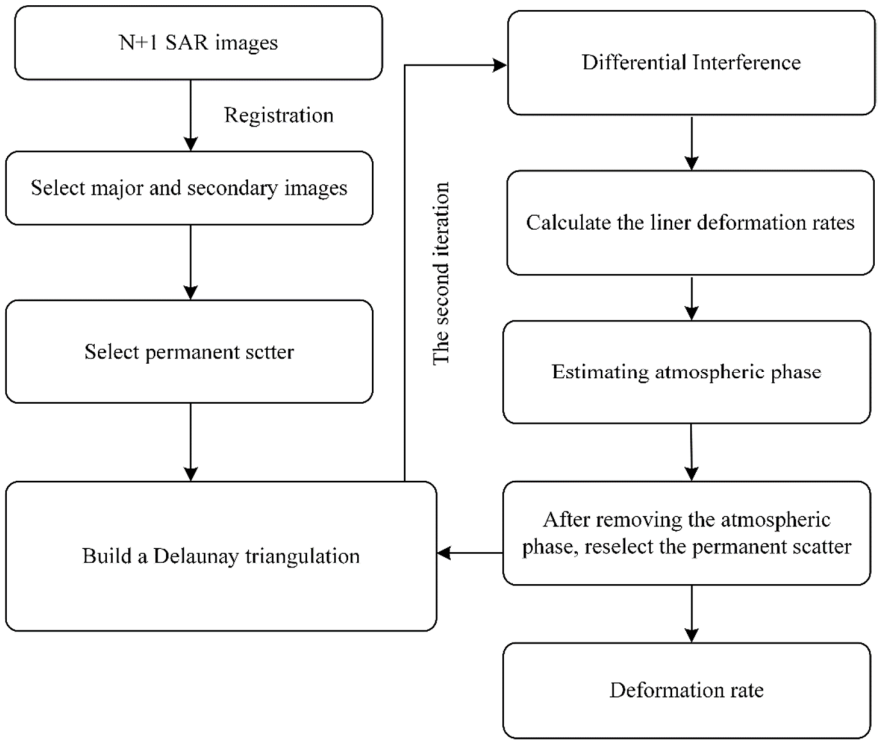

Figure 6. The framework of PS-InSAR analysis. The final deformation rate results of N + 1 SAR data are obtained by the flow in the figure.

In Figure 6, in the monitoring of GBSAR, the radar transmitter moves along a fixed orbit in each measurement. After the main image is selected, PS points are selected by setting thresholds for the phase dispersion index and coherence coefficient, and then the auxiliary image and the main image are subjected to interference processing, respectively, to construct a phase model function. Then, build a Delaunay triangulation for all adjacent PS points, use the solution space search method for the phase difference of PS points on the same baseline, iteratively solve the linear deformation rate, analyze the residual phase, and estimate the atmospheric phase component. After the atmospheric phase is separated from the phase, the PS point is reselected and the above operation is repeated to obtain the deformation time series results of the monitoring area.

3.2.2. Real-Time Processing

For time $t - 1$, use the scene data before $t - 1$ to analyze the time series of the monitoring area, and obtain the deformation variable data within this time range, and use

these data as the data set of the LSTM model to predict the deformation variable at time t. The meteorological parameters [30] collected by the weather station at the previous time $t-1$ are used to fit and predict the atmospheric phase at time t, which can be:

$$\varphi_{t\_pred} = \varphi_{atm\_pred} + \varphi_{def\_pred} \tag{16}$$

The formula represents the predicted phase at time t, including the predicted value of the atmospheric phase and the predicted value of the deformation phase. At time t, if you want to perform time series analysis, you need to remodel and solve the data at the previous time t, which will waste more time and resources. Interference is performed at time t, and the phase includes:

$$\varphi_t = \varphi_{atm} + \varphi_{def} + \varphi_{noise} + 2k\pi \tag{17}$$

The atmospheric phase change and deformation phase change at time t relative to time $t-1$ are subtracted from the difference result between time $t-1$ and time t. At this time, there are only residual atmospheric phase and residual deformation phase in the phase. bit and noise phase. At this time, the spatial domain unwrapping of the interference phase is performed after the spatial domain filtering, which is easier than the original differential phase, and a better unwrapping result can be obtained. After the unwrapped phase is obtained, according to the deformation result at time $t-1$, a mask is generated to cover up the area with a large deformation amount. For the stable area, the residual phase is the atmospheric phase of the area. The residual atmospheric phase of the entire monitoring area is obtained by interpolation, and the residual deformation phase can be obtained by subtracting the phase from the previous step. After being converted into a deformation variable and added to the predicted deformation variable at time t, the predicted deformation variable at time t can be corrected, and the time for time series analysis can be saved in order to achieve the effect of real-time monitoring.

4. Results

In this section, the GBSAR monitoring data of Guangyuan City, Sichuan Province were used for experiments, and 20% of the total data were used to predict the atmospheric phase and shape variables. Finally, 40 views of GBSAR data from 14:39 on October 28 to 03:59 on October 29 were used for the real-time processing experiment.

Figures 7 and 8, respectively, show the interferogram and the selected PS point diagram at 16:00 on the 17th and 16:00 on the 19th. Analysis of Figure 7 shows that the landslide body has undergone large deformation, and the coherence is poor in the vegetation coverage area.

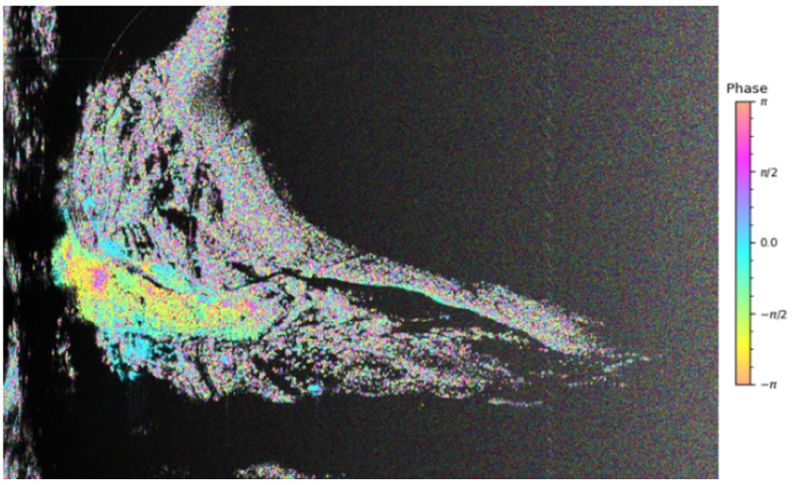

Figure 7. Interferogram result between 16:00 on the 17th and 16:00 on the 19th.

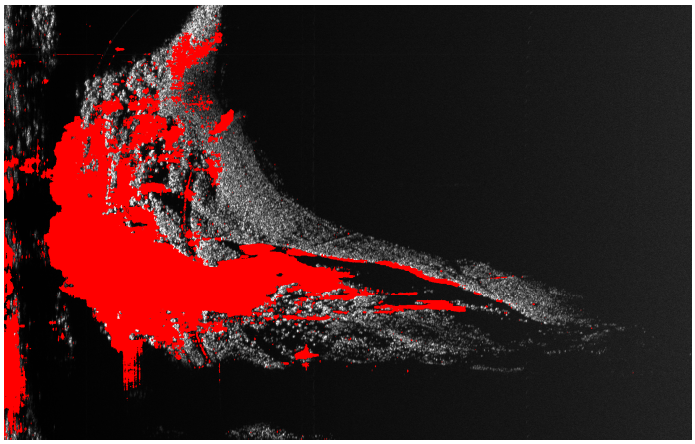

Figure 8. Schematic diagram of PS points selected in the target area.

4.1. Atmosphere Prediction

In this paper, the monitoring area was monitored for 16 days of meteorological parameters. By ensuring that the sampling frequency of GBSAR was consistent with that of GBSAR, the changes in atmospheric parameters during the observation period were obtained. According to the atmospheric phase model of GBSAR, the atmospheric phase based on the distance direction was obtained. The data set was constructed using this data, and the LSTM prediction result of the monitoring area was obtained by applying the LSTM network model, which is plotted in Figure 9.

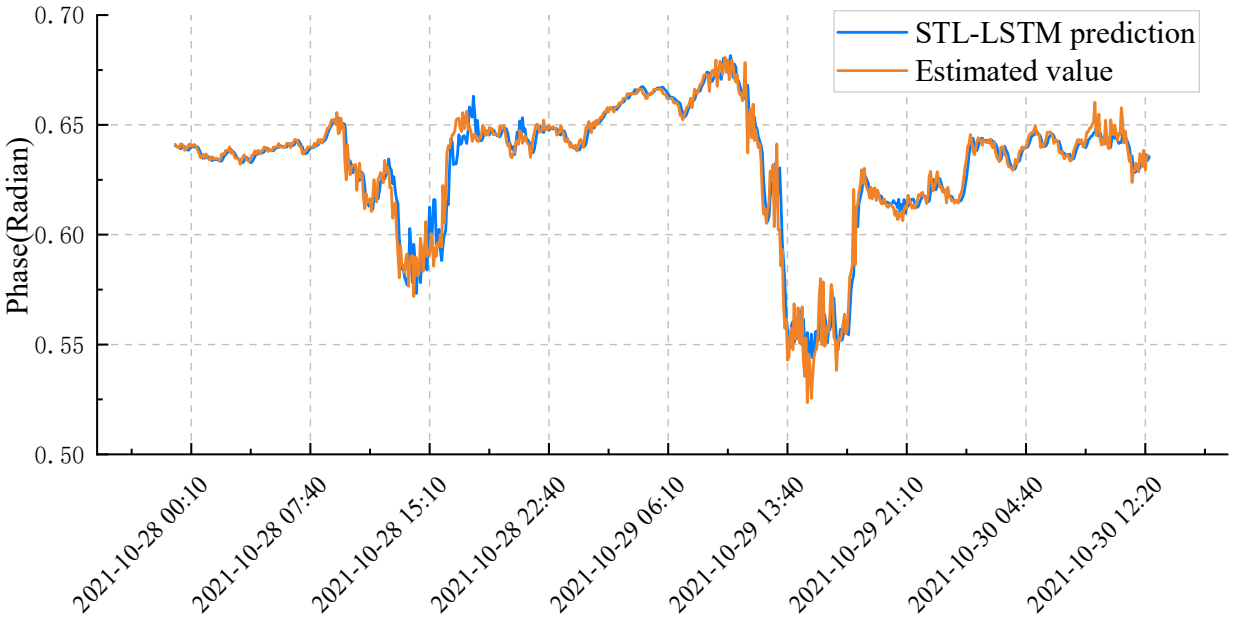

Figure 9. Time series change diagram of atmosphere phase prediction.

4.2. Deformation Prediction

In this paper, a total of 1,398,120 PS points and the deformation amount of 59 h in the entire monitoring area were predicted, and the deformation prediction results are partially shown in Figure 10 below according to a certain time interval. To make a difference, we drew the prediction residuals as shown in Figures 11 and 12, and drew the prediction residuals in Figures 13 and 14. By analyzing the above results, it can be seen that the LSTM network model has high prediction accuracy in the entire monitoring area, and the prediction results of the key deformation area and the stable area are in line with the facts.

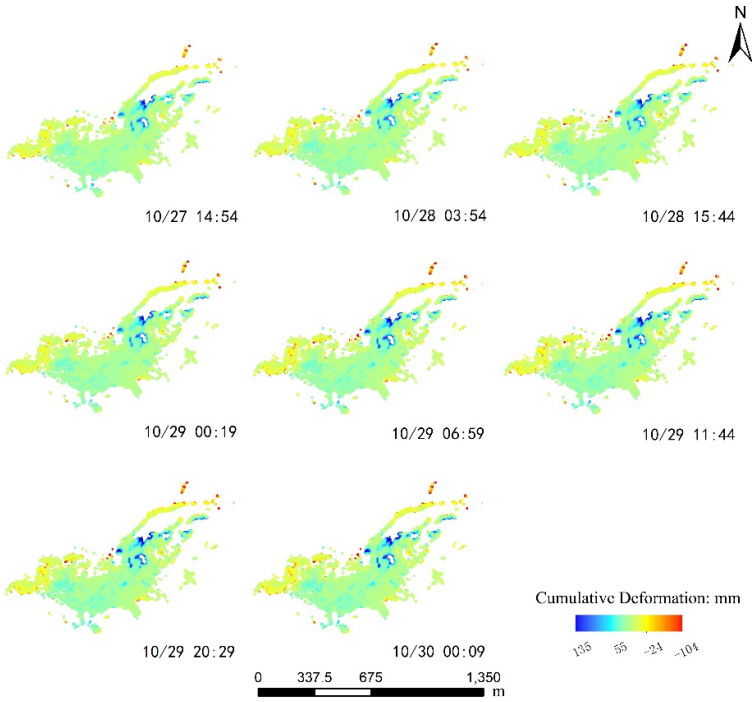

Figure 10. Historical results of deformation prediction along LOS direction. The displacement map was generated between the date that is marked in the low right corner and 17 October 2021 (the first acquisition date of GBSAR image). The deformation of the landslide is obvious. The color bar ranges from −104 mm to 135 mm.

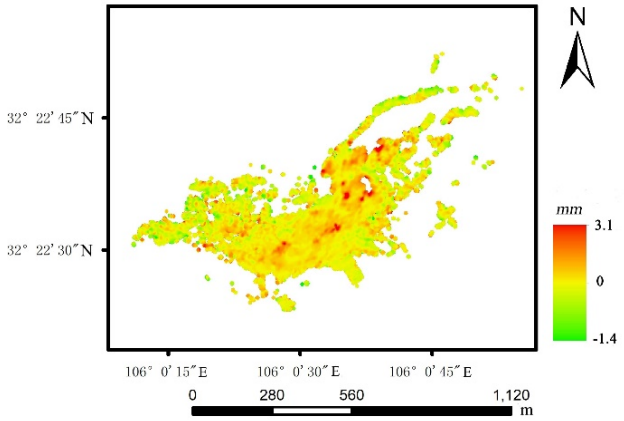

Figure 11. 10/29 20:29 Residual plot of real value and predicted value.

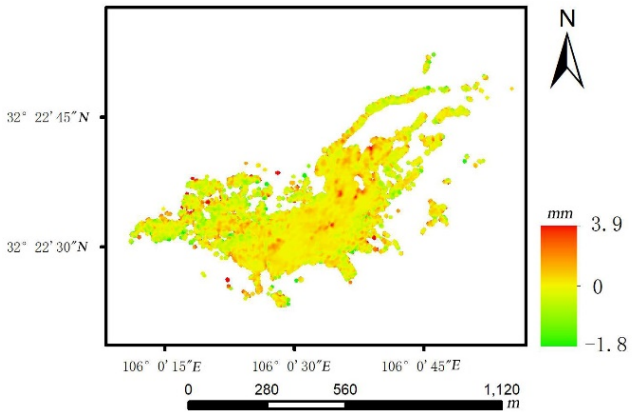

Figure 12. 10/30 00:09 Residual plot of real and predicted values.

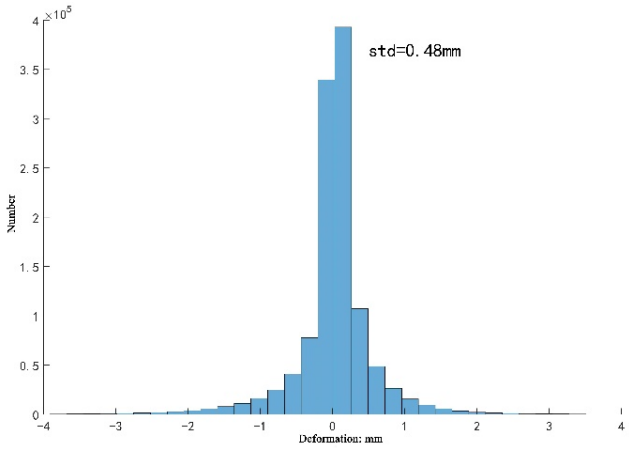

Figure 13. 10/29 20:29 residual histogram.

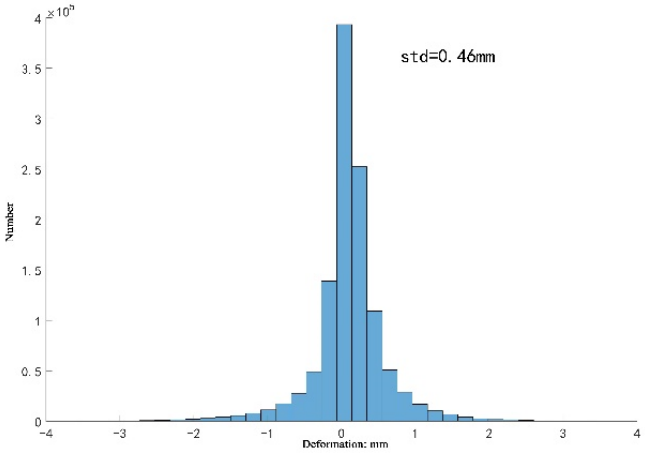

Figure 14. Histogram of residuals at 10/30 00:09.

4.3. Real-Time Processing

This experiment uses the ground-based SAR data of 40 scenes from 14:39 on 28 October to 03:59 on 29 October. First, the difference results between time $t-1$ and time t are obtained as shown in Figure 15. From the difference map, it can be clearly seen that there is an atmospheric phase with a trend term, and there is relatively large atmospheric disturbance in the area farthest from the radar center. The atmospheric phase and deformation phase predicted by the LSTM model are subtracted from the interference phase, and the results are shown in Figure 16. Analysis of the results shows that when fitting the atmospheric phase in the horizontal direction in this area, there is still atmospheric turbulence in the elevation direction and in a small area. For this part of the atmospheric phase, the method of mask interpolation after unwrapping is used to remove it. For the phase residuals of adjacent moments, spatial domain filtering is first performed, and the filtering results are shown in Figure 17. The filtering will remove the noise interference in the residuals. After that, the minimum cost flow method is used to unwrap, and the unwrapping results are shown in Figure 18. After unwrapping, the atmospheric phase of the trend term can be clearly seen, and then the stable region is interpolated after masking, and the fitted atmospheric phase is shown in Figure 19. After subtracting the residual atmospheric phase from the residual, the residual deformation is obtained as shown in Figure 20. Analysis of Figure 18 shows that the residual deformation of most regions is predicted to be zero, which proves that the LSTM model can be used to complete large regions with high accuracy. In the deformation prediction, the real-time processing deformation variable at time t is obtained by adding the deformation residual to the predicted value at the end.

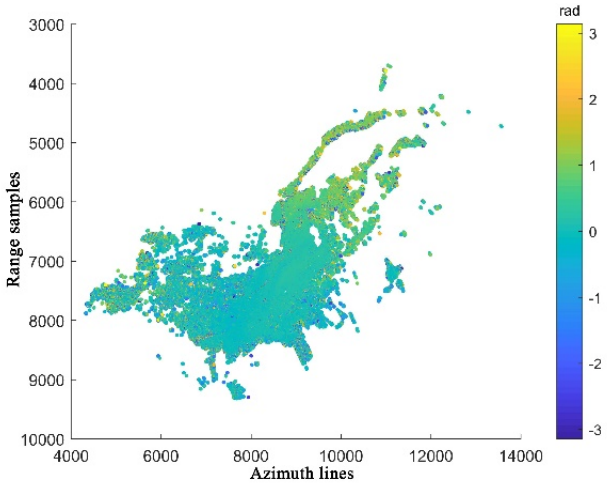

Figure 15. Interferogram of adjacent images. The interference phase includes the deformation phase, atmospheric phase, noise and whole cycle.

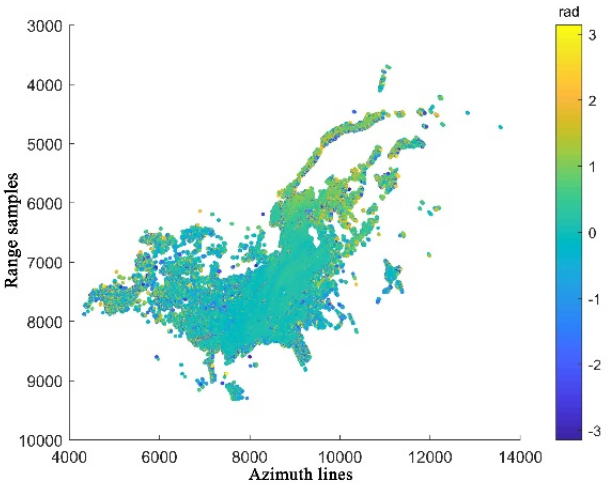

Figure 16. Interferogram residual phase diagram. The phase includes the remaining deformation phase, the remaining atmospheric phase and the whole cycle.

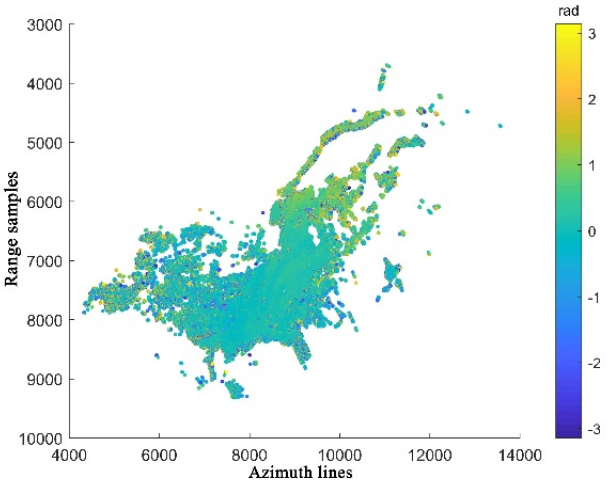

Figure 17. Residual phase map after filtering. The residual phase is filtered by the spatial domain filtering algorithm, and the filtered phase is obtained.

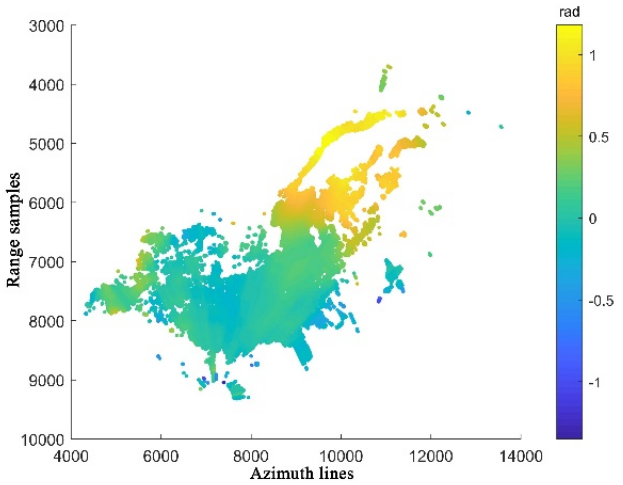

Figure 18. Residual phase diagram after unwrapping. The interference phase contains only a small amount of deformation phase and atmospheric phase, so it is easier to untangle and reduce the unwinding error.

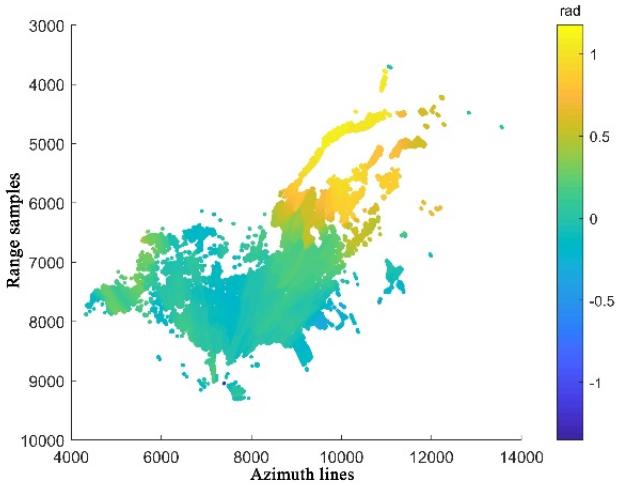

Figure 19. Interpolated atmospheric phase diagram. In the study area, the stable region is selected by taking the shape variable as the threshold, and the phase of the stable region is interpolated to obtain the overall atmospheric delay phase.

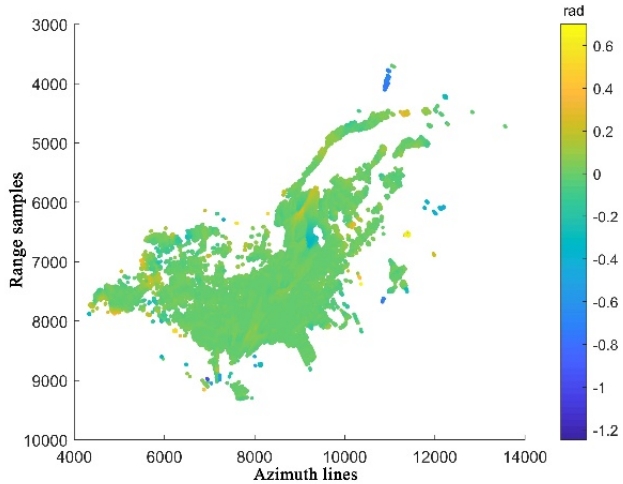

Figure 20. Residual deformation phase diagram. The residual deformation phase can be calculated by subtracting the interpolated atmospheric phase from the residual.

By processing 40 scene data to simulate real-time processing in the monitoring environment, the final deformation rate graph is obtained as shown in Figure 21:

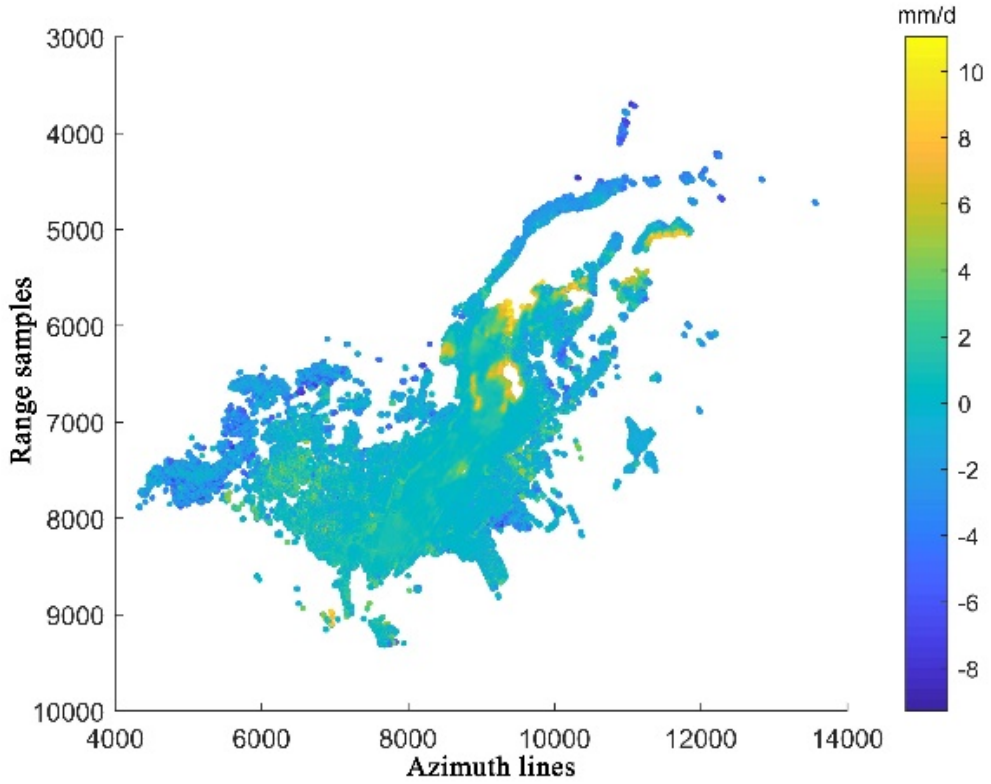

Figure 21. Final deformation rate graph. The slide body can be clearly identified from the figure and the deformation of the slide body can be analyzed.

According to the points P1, P2 and P3 selected in Figure 1a, they are used as the research objects for time series analysis, and their time series change curves within 800 min are drawn as shown in Figures 22 and 23:

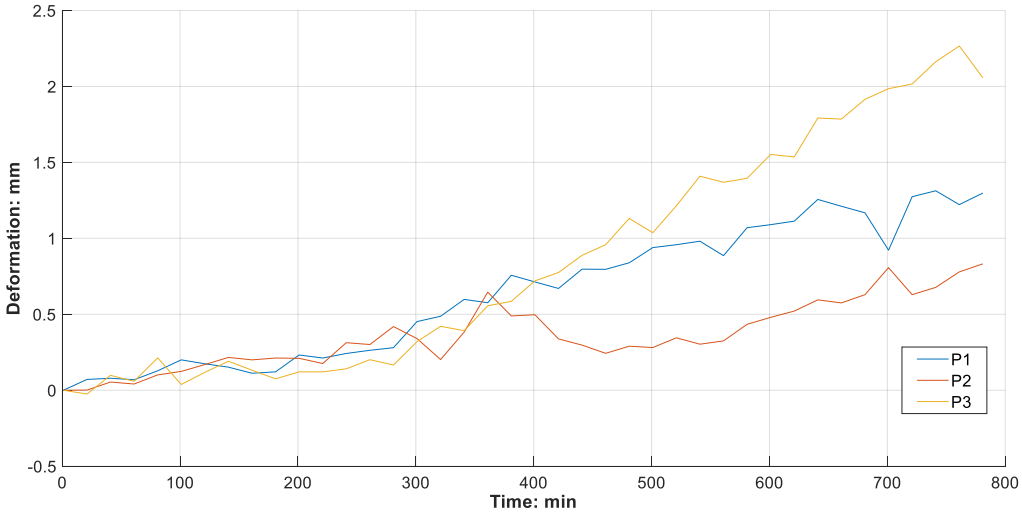

Figure 22. Real deformation curves of three research points. P1 is located at the crown cracks, P2 is located at the head, and P3 is located at the minor scarp. According to the analysis curve, the deformation rate of the three points is different, but all of them keep rising.

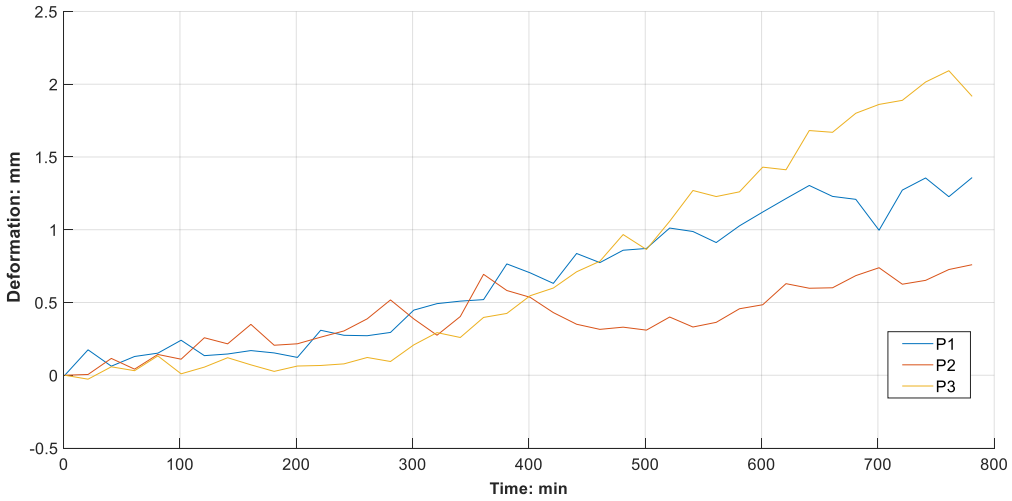

Figure 23. Real time processing method for deformation curves.

By analyzing the change curves of the three points in Figure 23, the time series results obtained by this real-time processing method are consistent with the GB-InSAR time series analysis results, which are in line with the real deformation variable changes, which proves that this method can realize real-time deformation processing. The process is as follows: select the deformation variable in the stable region for statistical analysis, and draw the frequency statistical histogram of the deformation variable in this region as shown in Figure 24:

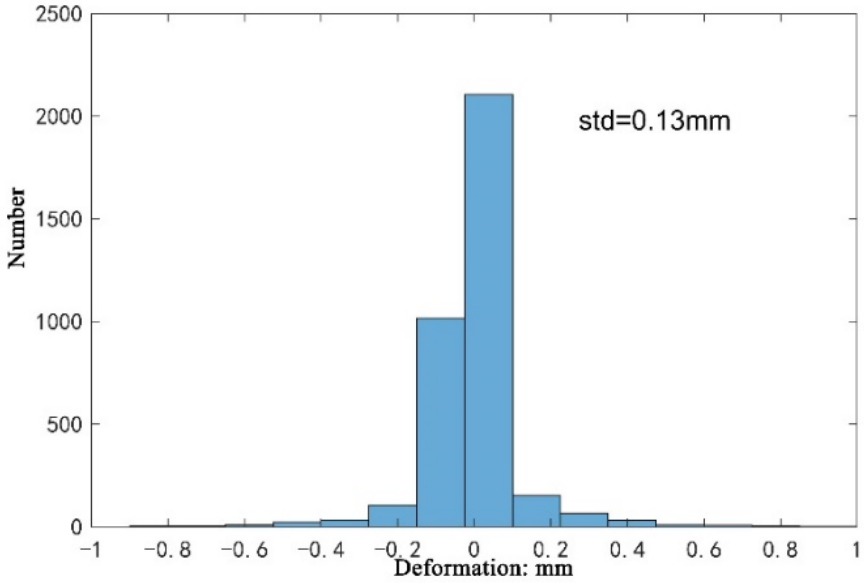

Figure 24. Deformation statistics histogram of the real-time processing method.

Generally speaking, the GB-INSAR deformation results need to be obtained through timing processing. Timing processing requires modeling and analysis of the entire data, using PS-InSAR or SBAS-InSAR methods. Due to the large amount of data in this method, the processing needs a lot of time, and the data set needs to be recalculated every time an additional scene is added. In this paper, the time of sequence analysis of 40 scenes of GBSAR data is counted, and the computer configuration used in the experiment is shown in Table 5. The time consumed by the real-time processing method proposed in this paper is plotted in Table 6.

Table 5. Experimental environment configuration.

Operating System	**Ubuntu 20.04**
Development Platform	Google Tensorflow
GPU	TITAN RTX 32G
CPU	Inter Xeon(R) Silver 4116 @2.10GHz × 48
Memory	128G

Table 6. Time-consuming statistics table.

Number of Data Scenes	**33**	**34**	**35**	**36**	**37**	**38**	**39**	**40**
Consume Time (min)	4.72	4.77	4.75	4.7	4.76	4.71	4.71	4.73
Original Time (min)	35.4	35.4	35.4	35.5	35.5	35.5	35.6	35.6

According to Table 5, GB-InSAR real-time monitoring based on LSTM network model has high processing efficiency, which can realize real-time monitoring and obtain high-precision results in slope monitoring. The average time of obtain deformation results by the real-time processing method is 4.73 min, which is much faster than the ordinary time series processing method. It is proved that the method can obtain results quickly and play a greater role in site landslide monitoring.

5. Discussion

The results show that the application of the LSTM model can effectively predict the deformation variables of the landslide in Guangyuan City, Sichuan Province. By evaluating the accuracy of the prediction results, the results show that the LSTM model can provide accurate prediction results. Compared with the linear prediction model, using the LSTM model for prediction can mine the correlation between historical data and make more accurate predictions for future data; compared with the machine learning model, it has the advantages of faster model convergence and higher prediction accuracy. At the same time, the distance from the study area to the atmosphere was predicted, and good prediction results were also obtained. GB-InSAR technology has the advantages of high precision, high spatial and temporal resolution, and flexible observation. The combination of the LSTM model and GB-InSAR provides more means for ground observation.

Based on the LSTM model, the GB-InSAR real-time processing method proposed in this paper can complete the extraction of deformation information in a short time. In the case of fewer computer resources and shorter time consumption, GB-INSAR time series processing is completed, and the time series results of deformation variables are obtained. The method proposed in this paper can provide case reference and verification for subsequent GB-InSAR monitoring technology and data-processing methods.

6. Conclusions

As a non-contact measurement technology, GB-InSAR technology can measure landslides with high precision and high spatial and temporal resolution. Compared with SAR satellites, ground-based SAR has a short time baseline, no spatial baseline, high resolution, and high-resolution observation. The advantages of flexible angle are widely used in landslide monitoring. Based on this, this paper proposes a GB-InSAR timing processing method based on the LSTM network model, aiming at the importance of deformation prediction in GBSAR monitoring, and the shortcomings of GB-InSAR timing analysis, such as slow processing efficiency, high memory consumption and inability to carry out real-time monitoring. The experimental results show that the method can quickly obtain the deformation prediction results in the monitoring area, and the inner coincidence accuracy evaluation proves that the method has high deformation prediction accuracy. At the same

time, the real-time processing module can obtain the shape variables in real time, and the hardware occupancy rate is low, which proves that the method has high-precision real-time processing ability. The following conclusions are drawn through the experiment:

(1) The LSTM model has high deformation prediction accuracy for the deformation results of GB-InSAR, and the standard deviation of the deformation prediction residual is 0.46 mm, which has the advantages of high prediction accuracy and fast model convergence speed.

(2) The proposed method can quickly obtain deformation results without occupying a large amount of memory, and the real-time processing time of a single scene is better than 5 min.

(3) Compared with the traditional GB-InSAR time series processing method, the standard deviation of the proposed method in the slow deformation region is between 0.1–0.3 mm, and the average deviation from the traditional method is within 0.13 mm.

Author Contributions: All authors contributed to the study conception and design. Material preparation, data collection and analysis were done by J.H., H.Y., Y.L., Z.L., K.Z. and R.J. The first draft of the manuscript was written by J.H. and all authors commented on previous versions of the manuscript. All authors have read and agreed to the published version of the manuscript.

Funding: This research was funded by the National Natural Science Foundation of China (42174026), and the National Key Research and Development Program of China (2021YFE011004).

Data Availability Statement: Not applicable.

Acknowledgments: We thank the good advice and comments from anonymous reviewers to help improve the quality of the paper.

Conflicts of Interest: The authors declare no conflict of interest.

References

1. Lingua, A.M.; Piatti, D.; Rinaudo, F. Remote monitoring of a landslide using an integration of GB-INSAR and LIDAR techniques. In Proceedings of the 21st Congress of the International Society for Photogrammetry and Remote Sensing, Beijing, China, 25 June 2008.
2. Broussolle, J.; Kyovtorov, V.; Basso, M.; Ferraro, D.S.; Figueiredo, M.J.; Giuliani, R.; Oliveri, F.; Sammartino, P.; Tarchi, D. MELISSA, a new class of ground based InSAR system. An example of application in support to the Costa Concordia emergency. *ISPRS J. Photogramm. Remote Sens.* **2014**, *91*, 50–58. [CrossRef]
3. Emanuele, I.; Giovanni, G.; Massimiliano, N.; Luca, L.; Francesco, M.; Francesco, F.; Nicola, C. Sinkhole monitoring and early warning: An experimental and successful GB-InSAR application. *Geomorphology* **2015**, *241*, 304–314.
4. Calvari, S.; Di Traglia, F.; Ganci, G.; Giudicepietro, F.; Macedonio, G.; Cappello, A.; Nolesini, T.; Pecora, E.; Bilotta, G.; Centorrino, V.; et al. Overflows and Pyroclastic Density Currents in March-April 2020 at Stromboli Volcano Detected by Remote Sensing and Seismic Monitoring Data. *Remote Sens.* **2020**, *12*, 3010. [CrossRef]
5. Barla, M.; Antolini, F. An integrated methodology for landslides' early warning systems. *Landslides* **2016**, *13*, 215–228. [CrossRef]
6. Kuraoka, S.; Nakashima, Y.; Doke, R.; Mannen, K. Monitoring ground deformation of eruption center by ground-based interferometric synthetic aperture radar (GB-InSAR): A case study during the 2015 phreatic eruption of Hakone Volcano. *Earth Planets Space* **2018**, *70*, 181. [CrossRef]
7. Di, T.F.; Nolesini, T.; Ciampalini, A.; Solari, L.; Frodella, W.; Bellotti, F.; Fumagalli, A.; Rose, G.D.; Casagli, N. Tracking morphological changes and slope instability using spaceborne and ground-based SAR data. *Geomorphology* **2018**, *300*, 95–112.
8. Carla, T.; Tofani, V.; Lombardi, L.; Raspini, F.; Bianchini, S.; Bertolo, B.; Thuegaz, P.; Casagli, N. Combination of GNSS, satellite InSAR, and GB-InSAR remote sensing monitoring to improve the understanding of a large landslide in high alpine environment. *Geomorphology* **2019**, *335*, 62–75. [CrossRef]
9. Carla, T.; Gigli, G.; Lombardi, L.; Casagli, N. Monitoring and analysis of the exceptional displacements affecting debris at the top of a highly disaggregated rockslide. *Eng. Geol.* **2021**, *294*, 106345. [CrossRef]
10. Dario, P.; Luisa, O.; Gianfranco, N.; Michele, C.; Jordi, R.; Pere, B.; Marc, J. Investigating the kinematics of the unstable slope of Barberà de la Conca (Catalonia, Spain) and the effects on the exposed facilities by GBSAR and multi-source conventional monitoring. *Landslides* **2021**, *18*, 457–469.
11. Long, S.; Tong, A.; Yuan, Y.; Li, Z.; Wu, W.; Zhu, C. New Approaches to Processing Ground-Based SAR (GBSAR) Data for Deformation Monitoring. *Remote Sens.* **2018**, *10*, 1936. [CrossRef]
12. Martinez, A.; Aguasca, A.; Lort, M.; Broquetas, A. Micrometric deformation imaging at W-Band with GBSAR. *Eur. J. Remote Sens.* **2016**, *19*, 719–733. [CrossRef]

13. Crosetto, M.; Monserrat, O.; Luzi, G.; Cuevas-Gonzá, M.; Devanthéry, N. Discontinuous GBSAR deformation monitoring. *ISPRS J. Photogramm. Remote Sens.* **2014**, *93*, 136–141. [CrossRef]
14. Wang, Y.; Zhang, Q.; Lin, Y.; Zhao, Z.; Li, Y. Multi-Phase-Center Sidelobe Suppression Method for Circular GBSAR Based on Sparse Spectrum. *IEEE Access* **2020**, *8*, 133802–133816. [CrossRef]
15. Wang, Z.; Li, Z.; Mills, J. Modelling of instrument repositioning errors in discontinuous Multi-Campaign Ground-Based SAR (MC-GBSAR) deformation monitoring. *ISPRS J. Photogramm. Remote Sens.* **2019**, *157*, 26–40. [CrossRef]
16. Wang, Z.; Li, Z.; Liu, Y.; Peng, J.; Mills, J. A New Processing Chain for Real-Time Ground-Based SAR (RT-GBSAR) Deformation Monitoring. *Remote Sens.* **2019**, *11*, 2437. [CrossRef]
17. Izumi, Y.; Zou, L.; Kikuta, K.; SATO, M. Iterative Atmospheric Phase Screen Compensation for Near-Real-Time Ground-Based InSAR Measurements Over a Mountainous Slope. *IEEE Trans. Geosci. Remote Sens.* **2020**, *58*, 5955–5968. [CrossRef]
18. Liu, Q.; Zhang, Y.; Deng, M.; Wu, H.; Kang, Y.; Wei, J. Time series prediction method of large-scale surface subsidence based on deep learning. *Acta Geod. Cartogr. Sin.* **2021**, *50*, 396–404.
19. Yang, H.; Peng, J.; Cui, H. Slope of Large-scale Open-pit Mine Monitoring deformations by Using Ground-Based interferometry. *Prog. Geophys.* **2012**, *27*, 1804–1811.
20. Liu, J. *The Research of Atmospheric Correction Method for GB-InSAR*; China University of Geosciences: Beijing, China, 2020.
21. Rödelsperger, S.; Läufer, G.; Gerstenecker, C.; Becker, M. Monitoring of displacements with ground-based microwave interferometry: IBIS-S and IBIS-L. *J. Appl. Geod.* **2010**, *4*, 41–54. [CrossRef]
22. Zhao, X.; Lan, H.; Li, L.; Zhou, C. A Multiple-Regression Model Considering Deformation Information for Atmospheric Phase Screen Compensation in Ground-Based SAR. *IEEE Trans. Geosci. Remote Sens.* **2020**, *58*, 777–789. [CrossRef]
23. Iannini, L.; Monti, G.A. Atmospheric Phase Screen in Ground-Based Radar: Statistics and Compensation. *IEEE Geosci. Remote Sens. Lett.* **2011**, *8*, 537–541. [CrossRef]
24. Yu, H. A Study on Information Extraction of Water Body with the Modified Normalized Difference Water Index (MNDWI). *Natl. Remote Sens. Bull.* **2005**, *9*, 589–595.
25. Wantong, C.; Hailong, W.; Ren, S. CM-LSTM Based Spectrum Sensing. *Sensors* **2022**, *22*, 2286.
26. Jiao, F.; Huang, L.; Song, R.; Huang, H. An Improved STL-LSTM Model for Daily Bus Passenger Flow Prediction during the COVID-19 Pandemic. *Sensors* **2021**, *21*, 5950. [CrossRef] [PubMed]
27. He, J.; Wu, X.; Cheng, Z.; Yuan, Z.; Jiang, Y. DB-LSTM: Densely-connected Bi-directional LSTM for human action recognition. *Neurocomputing* **2021**, *444*, 319–331. [CrossRef]
28. Chaodong, F.; Li, Y.; Yi, L.; Xiao, L.; Qu, X.; Ai, Z. Multi-objective LSTM ensemble model for household short-term load forecasting. *Memetic Comput.* **2022**, *14*, 115–132.
29. Liu, Y. *Study on Monitoring Method of Surface Subsidence in Filling Mining Area Based on DS-InSAR*; China University of Mining and Technology: Beijing, China, 2021.
30. Du, J. *Application of Kalman Filtering in GB-InSAR Slope Deformation Monitoring*; China University of Geosciences: Beijing, China, 2021.